Supporting Information

Hierarchically porous magnetic Fe_3O_4/Fe-MOF used as effective platform for enzyme immobilization：kinetic and thermodynamic study on the structure-activity

Xia Gao,[a,b] Quanguo Zhai,[a] Mancheng Hu,[a] Shuni Li [a] and Yucheng Jiang*[a]

[a] Key Laboratory of Macromolecular Science of Shaanxi Province, School of Chemistry & Chemical Engineering, Shaanxi Normal University, Xi'an, 710062, P.R. China

[b] Shaanxi Key Laboratory of Comprehensive Utilization of Tailings Resources, Department of Chemical Engineering & Modern Materials, Shangluo University, Shangluo, 726000, P. R. China

* Corresponding author, Email: jyc@snnu.edu.cn

Experimental

Materials

Chloroperoxidase (CPO) was isolated from the growth medium of C. fumago according to the method established by Morris and Hager with minor modifications using acetone rather than ethanol in the solvent fractionation step. Then, CPO was further purified by DEAE-Sephadex A-50 ion exchange column chromatography. Horseradish peroxidase (HRP, EC 1.11.1.7) was purchased from Shanghai Xueman Biotechnology Co., Ltd and stored at minus 20 °C before use. 2,2-azino-bis(3-ethylbenzothiazoline-6-sulfonic acid) (ABTS) were purchased from Sigma–Aldrich (St. Louis, MO, USA) and stored at 0–4 ℃ before use. Trimesic acid (H_3BTC, 99%) was purchased from Alfa Aesar. Dimethyl formamide (DMF) was purchased from Tokyo Chemical Industry Co., Ltd. (Japan). Iron(III) chloride hexahydrate ($FeCl_3 \cdot 6H_2O$), ammonium acetate (NH_4Ac), sodium citrate, citric acid, ethylene glycol and zinc nitrate hexahydrate ($Zn(NO_3)_2 \cdot 6H_2O$, 99%) were purchased from Beijing Chemical Works (China). Hydrogen peroxide (30% in aqueous solution) was obtained from Xi'an Chemical Co. Ltd. All chemicals are of analytical grade unless otherwise indicated.

Measurements

N_2 adsorption-desorption measurements at 77 K were carried out using an automatic physical adsorption instrument (Micromeritics Instrument Corp, Atlanta, USA). The samples were firstly degassed at 150 ℃ for 12 h under vacuum. The pore size distribution and the total pore volume were derived according to the desorption branches of the isotherms using the BJH model analyses. The powder X-ray diffraction patterns (PXRD) were recorded on a Rigaku (Woodlands, USA) X-ray Powder Diffractometer equipped with a Cu sealed tube (λ = 1.5404

Å) with voltage at 40 kV, the current at 30 mA, the scanning speed at 1°·min^{-1}, and the scanning range setting at 5° to 80°. The morphologies of the samples were characterized by a field-emission scanning electron microscope (FESEM, Hitachi SU8220, Tokyo, Japan) and a field-emission transmission electron microscope (FETEM, Tecnai G2 F20, Hillsborough County, Florida, USA). Fluorescent tags of enzyme on Fe_3O_4/Fe-MOF composites were performed on a FV1200 laser scanning confocal microscope (Olympus, Beijing, China), by using fluorescein isothiocyanate (FITC) as fluorescent markers. Thermal analysis was performed on TA Q1000DSC thermoanalyzer systems under N_2 atmosphere. Ultraviolet-visible (UV-vis) absorption spectra of proteins were recorded using Perkin-Elmer Lambd 950 UV-vis spectrophotometer. The enthalpic and entropic changes of the enzyme catalytic reaction was measured by isothermal titration calorimetry (Nano ITC-Standard Volume, TA Instruments, New Castle, DE, USA). The interaction of enzyme with the support was investigated by using a thermal conductivity microcalorimeter (RD496-2000, Mianyang CP Thermal Analysis Instrument Co.Ltd).

The application of CPO/HRP-Fe_3O_4/Fe-MOF

The simulated wastewater was prepared by mixing the following components: 12000 mg·L^{-1} of glucose, 12000 mg·L^{-1} of starch, 3420 mg·L^{-1} of ammonium sulfate, 1680 mg·L^{-1} of K_2HPO_4, 33 mg·L^{-1} of $MgSO_4·7H_2O$, 15 mg·L^{-1} of sodium acetate, 240 mg·L^{-1} of $CaCl_2$, 120 mg·L^{-1} of $MnSO_4$, 70 mg·L^{-1} of peptone, and 1 mg·L^{-1} of $FeSO_4·7H_2O$.

The degradation of soluble antibiotics isoproturon or 2,4-dichlorophenol was carried out in simulated wastewater with total volume of 3 mL containing 2 mg CPO/HRP-Fe_3O_4/Fe-MOF and isoproturon or 2,4-dichlorophenol in the concentration range of 0-10 mmol·L^{-1}. The

reaction was started by adding H_2O_2 (0.1 mol·L^{-1}). After 15 min, the supernatant of the reaction mixture was extracted three times using ethyl acetate in interval 10 min. The combined organic extract was concentrated by rotary evaporation (0.09 Mpa, 35 ℃) to remove the extractant, and then dissolved in acetonitrile/methanol respectively and treated by 0.22 μm organic phase filtration membrane, then measured concentration of isoproturon and 2,4-dichlorophenol by HPLC (LC-20AT, Shimadzu). The mobile phase consisted of a mixture of acetonitrile and water (80:20, v/v, flow-rate gradient elution) for isoproturon and a mixture of methanol and water (60:40, v/v, flow-rate gradient elution) for 2,4-dichlorophenol. The flow rate was 0.5 mL·min^{-1} and the detector was set at 240 nm for isoproturon, while the flow rate was 1.0 mL·min^{-1} and the detector was set at 284 nm for 2,4-dichlorophenol, with the injection volume of 20 μL. All experiments were triplicated and data reported were mean values of three independent measurements.

Supplementary Figures

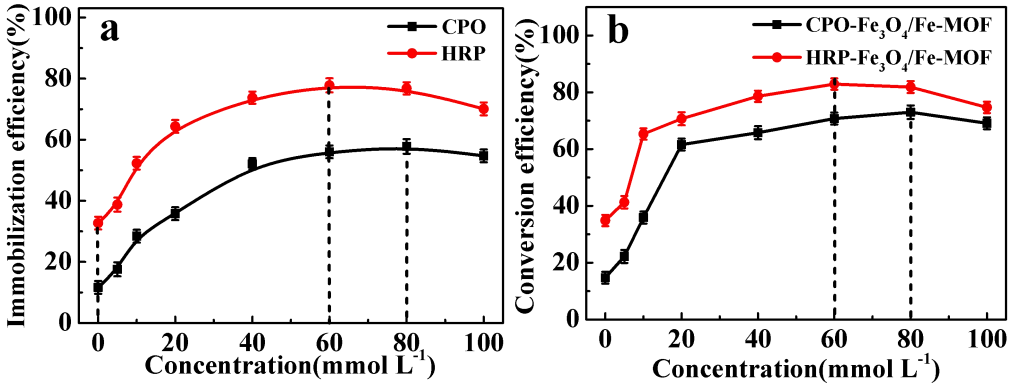

Fig. S1 The relationship between the concentration of Zn^{2+} solution and the enzyme immobilization efficiency (a) or the catalytic efficiency (b).

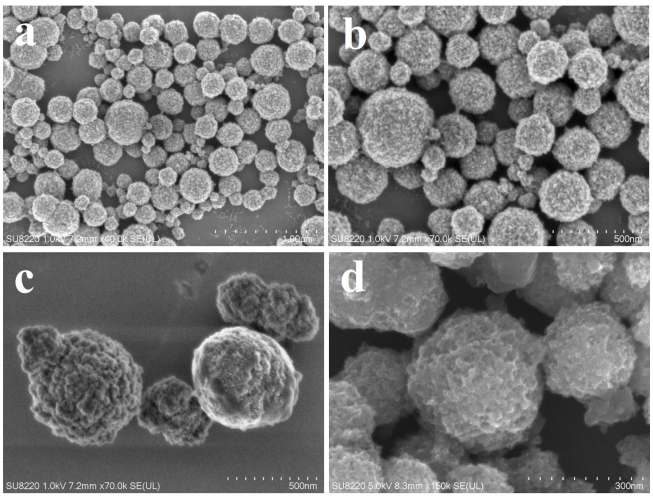

Fig. S2 FESEM images of Fe_3O_4 (a,b), Fe_3O_4/Fe-MOF (c) and CPO/HRP-Fe_3O_4/Fe-MOF (d).

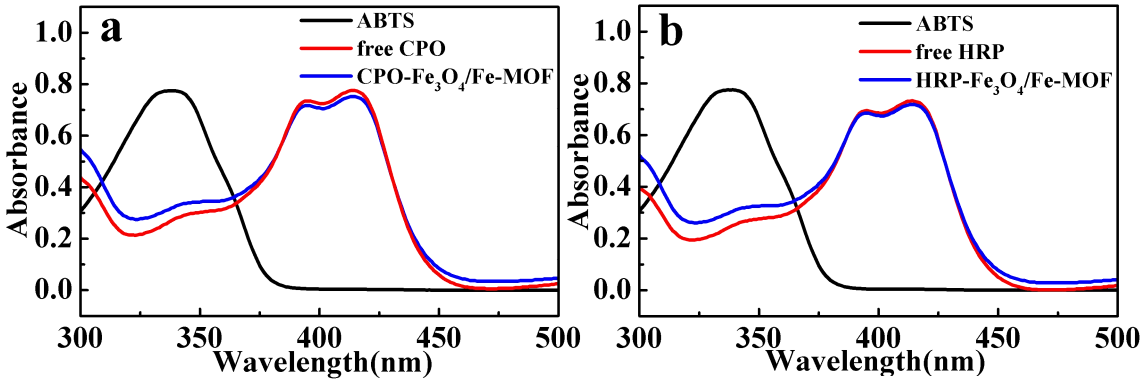

Fig. S3 UV-Vis absorbance spectra of peroxidation of ABTS catalyzed by free enzyme and CPO/HRP-Fe_3O_4/Fe-MOF: (a) CPO; (b) HRP.

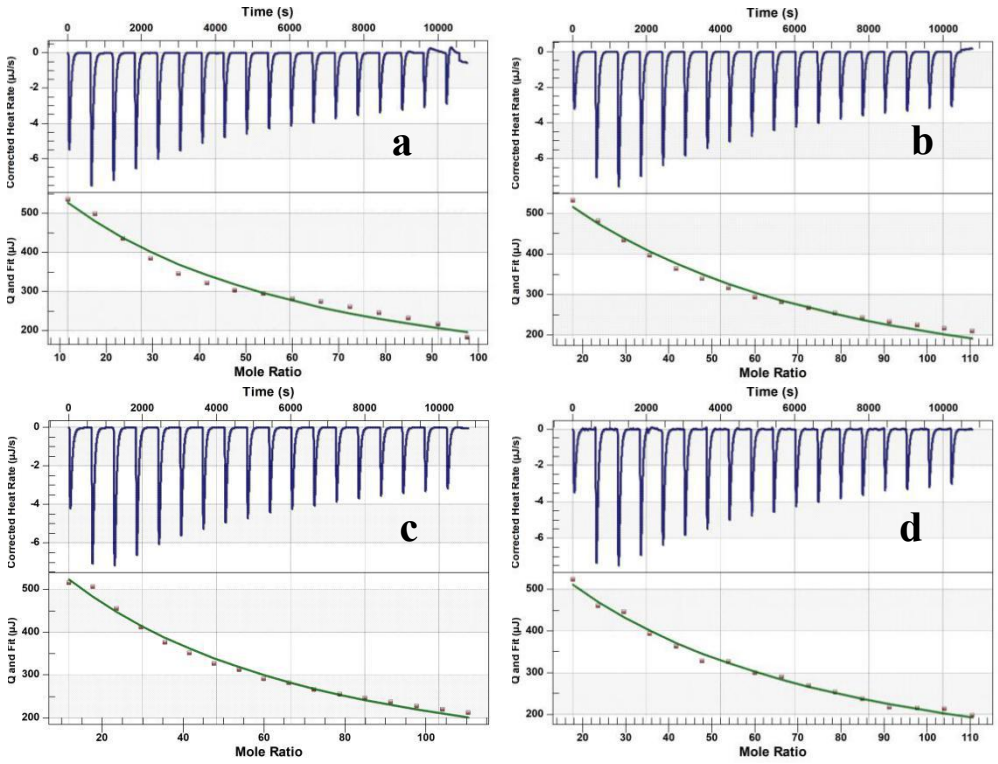

Fig. S4 Thermogram of raw heat and enthalpy with independent model fit for the isothermal titration of 10 mM ABTS into 0.01 mM enzyme: (a) CPO; (b) CPO-Fe_3O_4/Fe-MOF; (c) HRP; (d) HRP-Fe_3O_4/Fe-MOF.

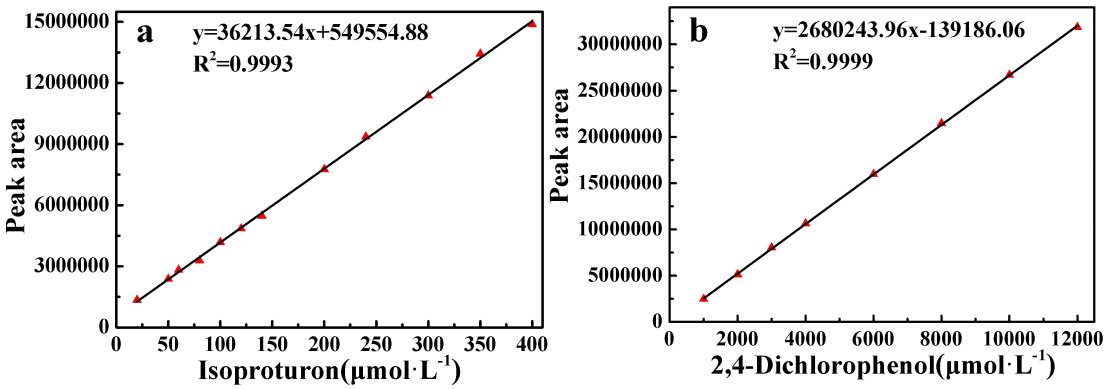

Fig. S5 The standard curves in determination of the substrates.

Supplementary Table

Table S1 Thermokinetic data of the preparation process of HRP-Fe_3O_4/Fe-MOF at different temperatures.

T/s	298.15 K			303.15 K			308.15 K		
	(H_t/H_∞)	In(1-H_t/H_∞)	In(dH_t/dt/H_∞)	(H_t/H_∞)	In(1-H_t/H_∞)	In(dH_t/dt/H_∞)	(H_t/H_∞)	In(1-H_t/H_∞)	In(dH_t/dt/H_∞)
10	0.9507	-0.0096	-6.5429	0.5960	-0.0060	-7.1168	0.5670	-0.0057	-6.9055
20	2.7465	-0.0278	-6.1218	1.5665	-0.0158	-6.7559	1.8976	-0.0192	-6.3807
30	5.2126	-0.0535	-5.8905	2.8466	-0.0289	-6.5540	3.8354	-0.0391	-6.1169
40	8.1647	-0.0852	-5.7594	4.3702	-0.0447	-6.4158	6.2077	-0.0641	-5.9713
50	11.4546	-0.1257	-5.6727	6.0870	-0.0628	-6.3155	8.8710	-0.0929	-5.8838
60	14.9829	-0.1623	-5.6202	7.9549	-0.0829	-6.2482	11.7288	-0.1248	-5.8308
70	18.6669	-0.2066	-5.5865	9.9325	-0.1046	-6.2028	14.7130	-0.1591	-5.7974
80	22.4517	-0.2543	-5.5675	11.9847	-0.1277	-6.1733	17.7786	-0.1958	-5.7779
90	26.2884	-0.3050	-5.5591	14.0919	-0.1519	-6.1503	20.8884	-0.2343	-5.7688
100	30.1460	-0.3588	-5.5577	16.2399	-0.1772	-6.1352	24.0171	-0.2747	-5.7664
110	33.9959	-0.4155	-5.5630	18.4155	-0.2035	-6.1262	27.1448	-0.3167	-5.7695
120	37.8213	-0.4752	-5.5711	20.6039	-0.2307	-6.1237	30.2571	-0.3604	-5.7765
130	41.6060	-0.5380	-5.5840	22.7956	-0.2587	-6.1226	33.3420	-0.4056	-5.7881
140	45.3398	-0.6040	-5.5986	24.9882	-0.2875	-6.1225	36.3859	-0.4523	-5.8027
150	49.0139	-0.6736	-5.6160	27.1788	-0.3172	-6.1259	39.3836	-0.5006	-5.8195
160	52.6234	-0.7470	-5.6341	29.3606	-0.3476	-6.1289	42.3266	-0.5504	-5.8395
170	56.1659	-0.8248	-5.6541	31.5423	-0.3790	-6.1246	45.2098	-0.6017	-5.8607
180	59.6357	-0.9072	-5.6757	33.7393	-0.4116	-6.1164	48.0294	-0.6545	-5.8842
190	63.0309	-0.9951	-5.6979	35.9500	-0.4455	-6.1131	50.7824	-0.7089	-5.9085
200	66.3499	-1.0892	-5.7206	38.1625	-0.4807	-6.1149	53.4676	-0.7650	-5.9340
210	69.5936	-1.1905	-5.7441	40.3682	-0.5170	-6.1198	56.0863	-0.8229	-5.9590
220	72.7619	-1.3006	-5.7672	42.5589	-0.5544	-6.1284	58.6369	-0.8829	-5.9869
230	75.8581	-1.4212	-5.7904	44.7299	-0.5929	-6.1379	61.1168	-0.9446	-6.0152
240	78.8817	-1.5550	-5.8145	46.8780	-0.6326	-6.1497	63.5270	-1.0086	-6.0439
250	81.8362	-1.7057	-5.8370	48.9993	-0.6733	-6.1631	65.8681	-1.0749	-6.0736
260	84.7222	-1.8788	-5.8609	51.0935	-0.7153	-6.1762	68.1399	-1.1438	-6.1040
270	87.5432	-2.0829	-5.8830	53.1580	-0.7584	-6.1907	70.3428	-1.2155	-6.1351
280	90.3009	-2.3331	-5.9057	55.1929	-0.8028	-6.2056	72.4774	-1.2902	-6.1673
290	92.9987	-2.6591	-5.9271	57.1958	-0.8485	-6.2221	74.5437	-1.3682	-6.2001
300	95.6385	-3.1324	-5.9487	59.1669	-0.8957	-6.2385	76.5443	-1.4501	-6.2319
310	98.2227	-4.0301	-5.9700	61.1055	-0.9443	-6.2544	78.4817	-1.5363	-6.2647

H_∞=-0.1917，-0.2797，-0.4884 J